Controlled synthesis of Zn^0 nanoparticles by bioreduction

G. Canizal [a], P.S. Schabes-Retchkiman [b], U. Pal [c], Hong Bo Liu [a], J.A. Ascencio [a,*]

[a] *Instituto Mexicano del Petroleo, Eje Central Lazaro Cárdenas No. 152, Col. San Bartolo Atepehuacan,*
Apartado Postal 14-805, C.P. 07730, México D.F., México
[b] *Instituto de Física, Universidad Nal. Autónoma de México, A.P. 20-364, C.P. 01000, México D.F., Mexico*
[c] *Instituto de Fisica, Universidad Autónoma de Puebla, Apdo. Postal J-48, Puebla, Pue. 72570, Mexico*

Abstract

Synthesis of metallic Zn nanoparticles through bio-reduction methods is reported for the first time. The structure, shape and size of the nanoparticles are critically controlled through the pH used in the sample preparation. High resolution electron microscopy was used in order to determine the structure of individual nanoparticles. Formation of quantum dots and the efficiency of ion reduction in the synthesis process are studied through the optical absorption in colloids. The structure and stability of the Zn clusters (up to 4000 atoms) were determined through the calculation of minimum energy configurations using molecular and quantum mechanics approximations and image simulation. The structure of the obtained nanoparticles was preferentially hexagonal, although multiple twinned and fcc-like structures were identified. The size controlled synthesis of small nanoparticles in the quantum-dot range was demonstrated successfully.
© 2005 Elsevier B.V. All rights reserved.

Keywords: Nanoparticles; Zinc; Bioreduction; Electron microscopy; Molecular simulation; Optical spectroscopy

1. Introduction

In recent times, the use of nanoparticles has become more generalized covering different fields including optoelectronics [1,2], catalysis [3,4], medicine [5] and sensor devices [6,7] among others. Three main parameters: structure, size and elemental composition [2,3], are considered to be very important besides the quantum size effects in the materials of nanometer scale, for possible applications. For instance, zinc has been vastly studied with focus on ZnO in sensors [6,7] and optical devices [1] due to the high selectivity of sensors and the semiconducting properties. Therefore, the synthesis of ZnO nanoparticles, one dimensional structures [6,7] and even the production of nanodisks [8], has been developed during the last few years. However, zinc metal (Zn^0) nanoparticles have not been studied enough, even when it has been demonstrated theoretically that they possess high stability and electronic structures revealing quantum size effects

in the nanometer size regime [9]. In fact, quantum mechanical calculations based on the density functional theory have demonstrated [9] that the gap between the highest occupied molecular orbital (HOMO) and the lowest unoccupied molecular orbital (LUMO) can vary from the bulk value of 0.27 eV to the highest of 4.59 eV for Zn_2 and 0.68 eV for Zn_{20}. However, there is no report of the gap values for bigger clusters which might behave differently in their optical and electrical properties.

Hence, the synthesis of size controlled Zn nanoparticles is quite important, especially in the size range of less than 3 nm, which to our knowledge, has not been reported yet. A previous work has reported the synthesis of monodispersed nanoparticles of around 17 nm [10], and others used precursors of diameters of 1–6 μm with no existing reports on quantum-dots synthesis. The synthesis methods reported until now are basically evaporation [8] and organometallic [10]. The bioreduction method, originally proposed by Gardea-Torresday for Au [11] and developed by our group to obtain Au nanorods [12], bimetallic nanoparticles [13] and even lanthanide clusters [14], is based on the use of the tannins of the biomass of *Medicago sativa* (alfalfa), and lately has

also been demonstrated effective for the synthesis of Au clusters using fungus [15]. The method is based on the reduction of metal ions through biomass at controlled pH conditions to improve the size control of nanoparticles.

As the size, shape and structure of the nanoparticles are very important, transmission electron microscopy (TEM) techniques are commonly used to determine the structure and local elemental composition [16] of nanomaterials. In the present work, we used a synthesis technique based on the bio-reduction method to obtain well size controlled zinc nanoparticles. Structure and stability of the particles are studied by TEM, molecular dynamics and quantum mechanical analysis. The use of optical spectroscopy allowed us to determine the efficiency of the method to reduce metal ions into nanoparticles [17,18]. The HOMO–LUMO gap of 0.33 eV for Zn_{38} and 0.04 eV for Zn_{85} demonstrate a high conductance in bigger zinc clusters, even better than many other metals.

2. Methods

Nanostructures of Zn were prepared using the bio-reduction method. In order to reduce Zn^{2+} ions to Zn^0 clusters, a similar path to that suggested by Gardea-Torresday et al. [11] and Ascencio et al. [13], for gold and Eu–Au nanoparticles is followed. A homogeneous suspension of powdered milled alfalfa (which had been washed previously, dried, milled, washed in HCl 0.01 M and dried again) was prepared with a concentration of 5 mg ml^{-1} in water using an ultrasonic treatment for 10 min. The pH of the solution was controlled by means of a buffer solution of the values between 3 and 10. After placing the mixture in an ultrasonic bath for 5 min, it was left for another 5 min without agitation and then centrifuged for 10 min. A zinc ion solution, 3×10^{-4} M of $(CH_3COO)_2Zn \cdot 2H_2O$ (where zinc had a II state of oxidation), prepared in deionized water. Both the solutions were mixed homogeneously using an ultrasonic bath for 20 min. Later, the mixture solution was kept at 25 °C for 1 h and centrifuged for 25 min. Finally, the reaction mixture was filtered and kept on rest for 48 h, after which they were used for optical and TEM characterizations.

For high resolution transmission electron microscopy (HRTEM) characterization, the samples were prepared by placing a drop of the solution on carbon-coated copper or nickel grids. Electron microscopy was performed in JEOL 4000EX and JEOL JEM-2010F FasTem Microscopes. High resolution images were obtained at the various defocus conditions for each microscope, including the optimal (Scherzer condition) [16].

In order to build the structural models, we used a geometry-based method to generate cubic (fcc-like), hexagonal (hcp-like) and decahedral (deca) structures. Their stability was evaluated using the DMol3 [19] method, based on the density functional theory (DFT) [20], which is a module of Cerius^2 of Accelrys. For the smallest clusters, we improved geometry optimization calculations with a local density approximation and the Perdew Wang functional [21] with a self consistent field tolerance of 1×10^{-6} Hartree, and with energy changes of 1×10^{-5} Hartree between optimization steps. For bigger clusters, we used a tight-binding potential with second-moment approximation (TB-SMA) as proposed by Tomanek et al. and Cleri and Rosato [22,23]. The potential has been smoothly truncated up to

the fifth neighbors in order to keep stable hcp structure for zinc. The molecular dynamics (MD) simulations were performed using XMD developed by Prof. J. Riffkin, Centers for Simulation, University of Connecticut, USA [24]. The program employs a predictor–corrector algorithm to integrate the equation of motion. In all the simulations reported here, a time step of 5×10^{-15} s was used, which is a fairly small value considering the temperature of 0 K. It was rather necessary to ensure the accuracy of energy calculations due to small energy difference among different isomers of Zinc.

The optical properties of the samples were studied by means of optical absorption spectroscopy. A Shimadzu UV-3101PC double beam spectrophotometer was used to record the optical absorption spectra of the samples in the 200–800 nm spectral range using deionized water as reference.

3. Results and discussion

Multiple samples were obtained by varying the pH from 3 to 6, which was considered to be the main variable in the present analysis. The samples prepared using different pH values (3–6) revealed significant differences between them. In all the cases Zn metallic nanoparticles were obtained. In order to determine the existence of Zn^0 atomic clusters, electron energy loss spectra were obtained. In Fig. 1(a), a typical EELS spectrum of the samples is shown where the shape and location of the plasmon peak clearly correspond to Zn^0. We can distinguish a sharp absorption signal due to the excitation of electrons from the 3d level at a binding energy of 9.4 eV and a relatively less pronounced and broad signal at about 14 eV as it was reported by Widder et al. [25]. The homogeneity of the cluster distribution can be determined with help of the high angle annular dark field (HAADF) contrast images [26]. In Fig. 1(b), a typical HAADF image produced by the particles is shown, where the clusters are quite homogeneous and the high contrast involves one kind of element, which must correspond to Zn as it is determined from the EELS spectrum. However, significant differences have been observed in size distribution, structure and shape of the clusters prepared with different pH values indicating a strong effect of the pH value in synthesis as expected and observed for other metallic clusters.

Fig. 2 is a composite figure, where a, b, c, d correspond to medium magnification TEM micrographs of the reduced zinc particles formed in the biomass for the pH values 3, 4, 5 and 6, respectively. To demonstrate the differences between the samples prepared for different pH values, a size distribution analysis was made considering over 150 nanoparticles for each sample. The measurement of size was performed along the largest diameter of the particles. The size distribution histogram, Fig. 2(e), shows clearly the main differences among the samples. Micrograph of Fig. 2(a) obtained for pH 3, shows a distribution of several sizes, from around 2 nm but mainly distributed around 5.6 nm. For the samples prepared with pH 4 (micrograph of Fig. 2(b)), the distribution is broader with a peak at about 3.5 nm. However, for pH 5 (refer Fig. 2(c)), the distribution peaked around 2.5 nm with
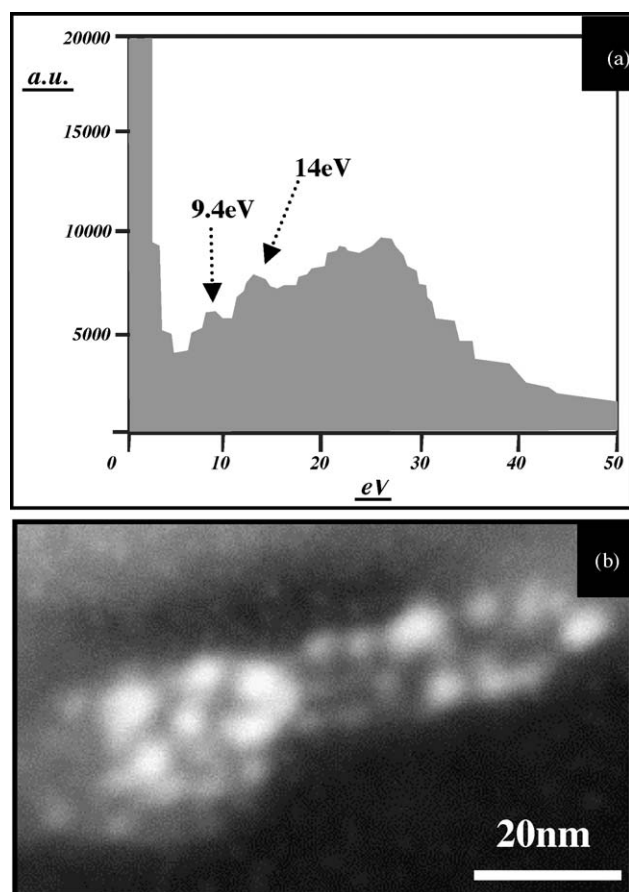
Fig. 1. Typical data of elemental composition for the samples. (a) Metallic zinc plasmon EELS, which corresponds to Zn^0 atoms; and (b) HAADF contrast image for Zn distribution in homogeneous clusters.

a narrow distribution and finally for pH 6 (refer Fig. 2(d)), the distribution becomes broader and no particular size was favored.

Therefore, the optimal size distribution, i.e. with the narrowest size and shape distribution and smaller clusters, was obtained for pH 5, where particles of small, regular in size and shape were formed. Therefore, the quantum size effects must be observed mainly in the samples produced with pH 5. However, it is also well established that beside the size, the corresponding structure of the particles is controlled by the surface energy in conjunction with the method of synthesis. Reduction of surface energy is controlled by the possible reactions and interaction of the particle surface with the passivating agents as has been reported while using thiols [27], or in this case, the tannins involved in the used biomass. So, it is important to determine the kind of structures formed in the samples. In order to study the lowest energy configurations for the clusters, a couple of calculations were made: quantum mechanics for the smallest clusters (8–55 atoms) and classical molecular mechanics for bigger configurations (110–4000 atoms). In Fig. 3, the quantum stability is plotted for the different configurations, for both quantum (3a) and classical (3b) approaches, while the modeled clusters used are

shown in 3c for the fcc-like, hcp-like and decahedral structures (two views of each are shown for clarity). In the first plot, it is clear that the three different structures are quite stable for the clusters of 8–38 atoms, where a few overlapping points indicate that the structures must coexist if the lowest energy can be achieved through the method of synthesis. The plots in Fig. 3(b) show that for bigger clusters the decahedral structure becomes more stable and those must be abundant if the synthesis process favors minimum energy configurations. However, the differences of energy among the structures are small and the synthesis process may produce all three kinds of nanoparticles. In fact, the differences in energy are so small that depending on the number of atoms, the production of each type of structure can be favored.

In order to determine the structure of the experimentally produced nanoparticles we analyzed HRTEM images, where the atomic columnar arrays are distinguished producing the characteristic contrast for each kind of cluster configuration. Due to the complexity in distinguishing these types of particle, we used simulated models (shown in Fig. 3(c)) to calculate the images of main orientations, which made the interpretation and contrast analysis easier. The calculated images can be observed in Fig. 4, where four images are shown for the considered configurations and based on the acceleration voltage, spherical aberration and Scherzer conditions of the used microscope (400 keV, $C_S = 1$ mm and $\Delta S = 40.5$ nm). The orientations are marked considering rotations over the Cartesian axes (considering x horizontal and y vertical, perpendiculars to the beam axis) in order to make the comparison easier even when their corresponding symmetries are quite different.

In Fig. 4(a) the structure shows the basic $\{0\,0\,1\}$ orientation with square dots arrays conventional for fcc-like systems; however, when the particle is rotated 45° in "x" the image shows a hexagonal distorted array of dots as it expected for the $\{1\,0\,1\}$ orientation. After an extra rotation of 35° in "y" the perfect hexagonal shape is reached ($\{1\,1\,1\}$ orientation). It must be noticed that because of the small inter-atomic distance, the contrast shows just a smooth central array of six elongated dots and an array of 12 white dots in the external zone but no further features are resolved. The image obtained after an extra rotation of 15° shows a contrast of fringes in the vertical direction. In Fig. 4(b), the corresponding images for the truncated hexagonal configuration, the characteristic contrasts are identified for the four images, starting with the $\{0\,0\,1\}$ that shows a hexagonal array of dots matching with the prediction for a common hcp crystal. Besides, when the cluster is rotated 45° around "x" ($\{1\,0\,1\}$ orientation) a rhombohedral contrast is defined retaining the hexagonal profile facets. The third image corresponds to a 90° rotation which produces a fringe contrast very similar to the observed in fcc-like clusters ($45x50y$), but when the particle is rotated 15° in "y", the obtained image shows a vertical zig–zag contrast and parallel lines in the horizontal direction. Finally, the decahedral particle (Fig. 4c) shows images similar to the images reported for other metals [16], with five triangles for five-fold
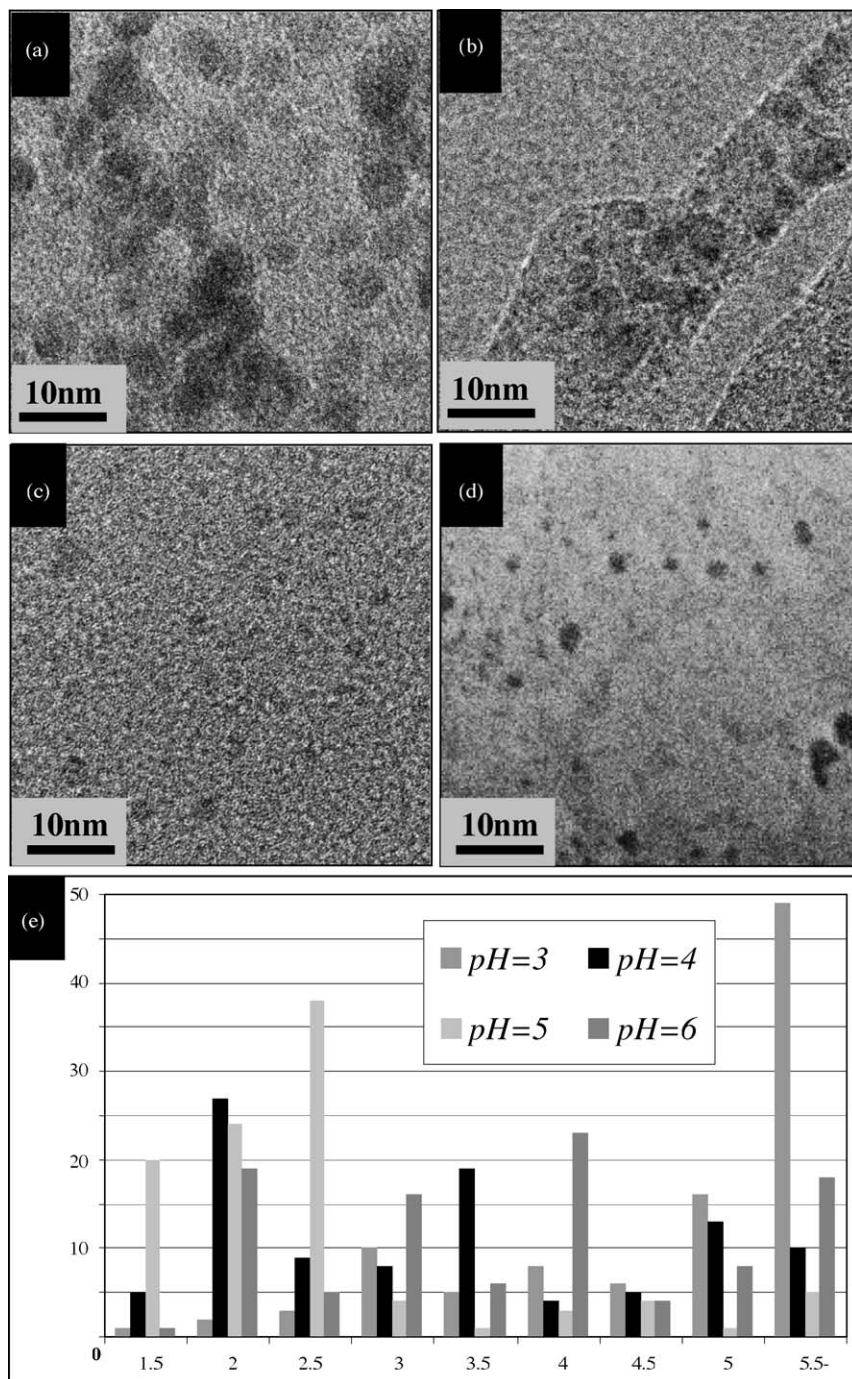
Fig. 2. Low magnification electron micrographs of the Zn nanoparticles obtained at pH values: (a) 3; (b) 4; (c) 5; (d) 6; and (e) the corresponding size distribution plots.

orientation and no homogeneous structure contrast in the left and right sides ($45x$ and $90x$), revealing vertical zig–zag contrast with no parallel lines for two-fold rotation ($90x90y$) as in the case of the hexagonal particle.

Fig. 5 shows three different examples of nanoparticle configurations observed in the samples prepared at pH 3, where a large amount of particles are obtained including zones with high concentration and cluster overlapping. However, as can be seen from Fig. 5(a), the structure and size of the particles are well defined. In this figure, we can see several particles, including an interesting central cluster with square dots distribution corresponds to fcc configuration in the $\{0\,0\,1\}$ orientation, which was not expected for the Zn bulk symmetry. The particle shown in Fig. 5(b) corresponds to a rounded structure with two zones of hexagonal contrast. The existence of a twin in the image is clearly revealed in the fast Fourier transform (FFT) that shows two hexagonal domains. Finally, in Fig. 5(c), a multiple twinned particle is identified with a
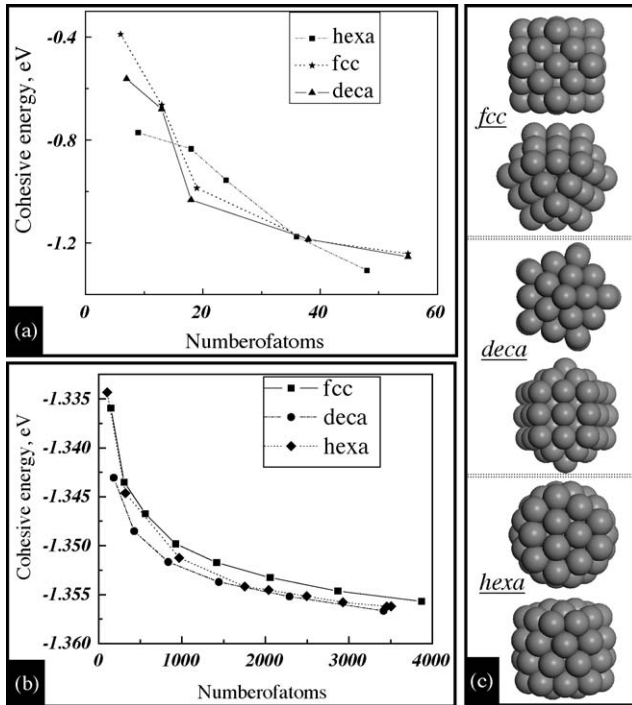
Fig. 3. Stability of Zn nanoparticles, calculated by: (a) quantum mechanics; and (b) classical mechanical approaches for clusters from 8–55 and 110–4000 atoms, respectively; with (c) the models of cubic (fcc) hexagonal (hcp) and decahedral (deca) structures used in the calculations and shown in two views for clarity.

contrast that matches with the five-fold {0 0 1} orientation of the decahedral configuration.

In the case of the samples obtained at pH 4, well-defined particles are observed. In Fig. 6(a), a couple of particles of diameters of 2.2 and 4.1 nm with hexagonal contrast are observed. In Fig. 6(b), a long cluster with irregular profile denotes the coalescence of three particles of 2.1, 3.8 and 3 nm, with small rotations between them generating mainly a rhombic contrast and sharing this alignment. This behavior of alignment when smaller particles coalesce to form a bigger aggregate has been previously reported for gold [28,29].

On analyzing the samples obtained with pH 5 (Fig. 7), three different types of particles with different configurations are observed. The first particle (Fig. 7(a)) of 2.2 nm size revealed fringe contrast including a few well define dots identifying as rhombohedral contrast with an FFT pattern associated to hexagonal particles. In the second particle (Fig. 7(b)) the contrast matches directly to the {0 0 1} orientation of a hexagonal particle. However, in the third particle (Fig. 7(c)), a multiple parallel twin particle is observed, denoting the multiple domains in the image and the lines of closely spaced dots in the FFT as has been observed for other metals [30].

Finally, samples obtained with pH 6 show a high size dispersion including the evidence of particles coalescence that generate nanorods (Fig. 8). In Fig. 8(a) and (b), a couple of hexagonal clusters with {0 0 1} and {0 1 1} orientations and their corresponding FFTs are shown. Fig. 8(c) shows multiple particle contrast in different orientations and shapes, revealing mainly a nanorod with internal twins almost perpendic-
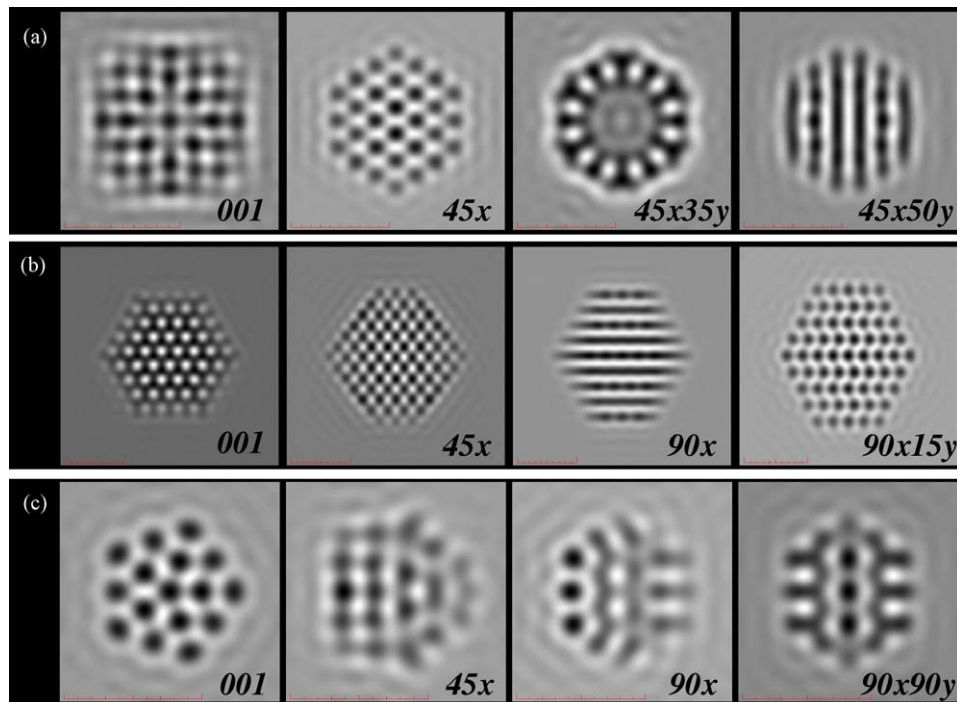
Fig. 4. HRTEM simulated images for: (a) fcc-like; (b) truncated hexagonal; and (c) pentagonal clusters. Four different orientations are shown for a better interpretation (rotation degrees are shown for each).
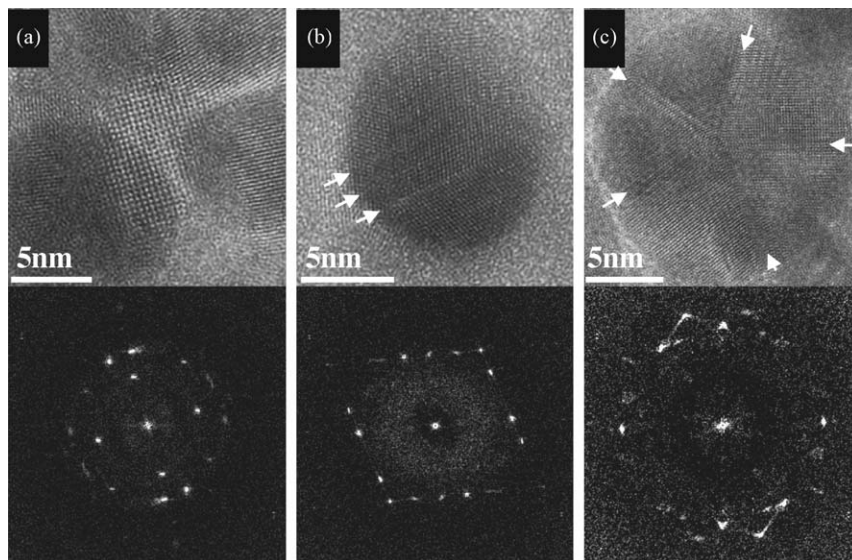
Fig. 5. HRTEM images of particles observed in samples of pH 3, where (a) square; (b) fringes; and (c) pentagonal contrast (see the twins marked by the arrows) are observed with their corresponding FFT for each image.

ular to the growth direction (axis). Though this behavior has been studied for other metals, no such observation is reported for Zn.

In this way, it can be established that the nanoparticles of different configurations can be obtained mainly for pH 3 and 6; while for pH 4 and 5, the particles produced have no defect configurations.

In order to understand the effect of the remaining ions in the synthesis of Zn^0 in the samples, we used an optical absorption evaluation in the range of 200–355 nm wavelength, where the presence of ions would be evident [17]. In the Fig. 9(a), the absorbance spectra show clearly that for pH values 3 and 4, the samples contain a large amount of free Zn^{2+} ions; while for pH 5, the absorption band of free ions (at about 280 nm) is reduced to the 25% and for the pH 6, it is the minimum being just 8% of the intensity of the corresponding absorption for the sample prepared with pH 3. These analyses allow us to understand the efficiency of the reduction method and its effect on the generation of a specific type of nanoparticle.

In Fig. 9(b), the absorption spectra of the samples in the 330–550 nm spectral range are shown, to demonstrate the formation of quantum dots in them. The absorption band appeared at about 335 nm is related to the formation of small Zn^0 clusters generally referred as surface plasmon resonance (SPR) absorption. Higher intensities of the SPR bands for
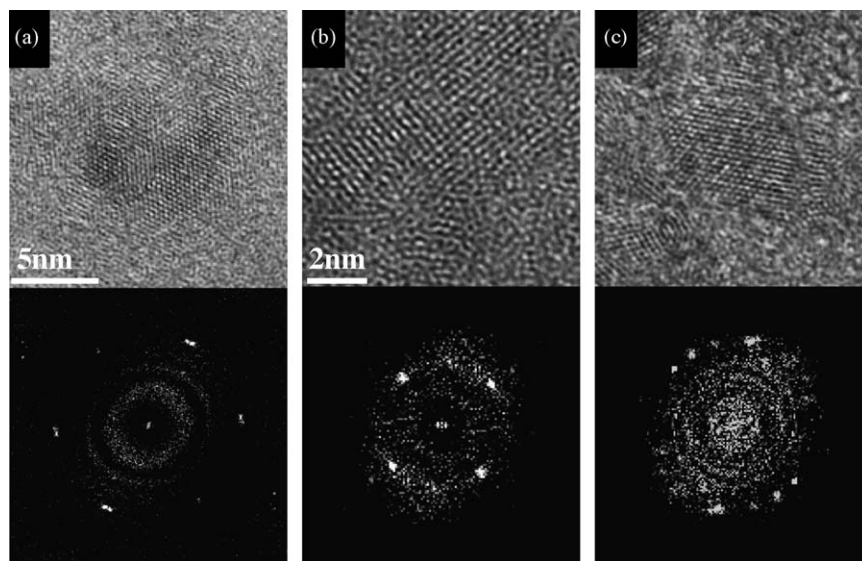
Fig. 6. HRTEM images of particles in the samples prepared with pH 4, where we can see three almost similar particles with fringe contrasts. However, the FFT's denote extra dots that allow to associate them to rhombic arrays characteristics for the hexagonal particles.
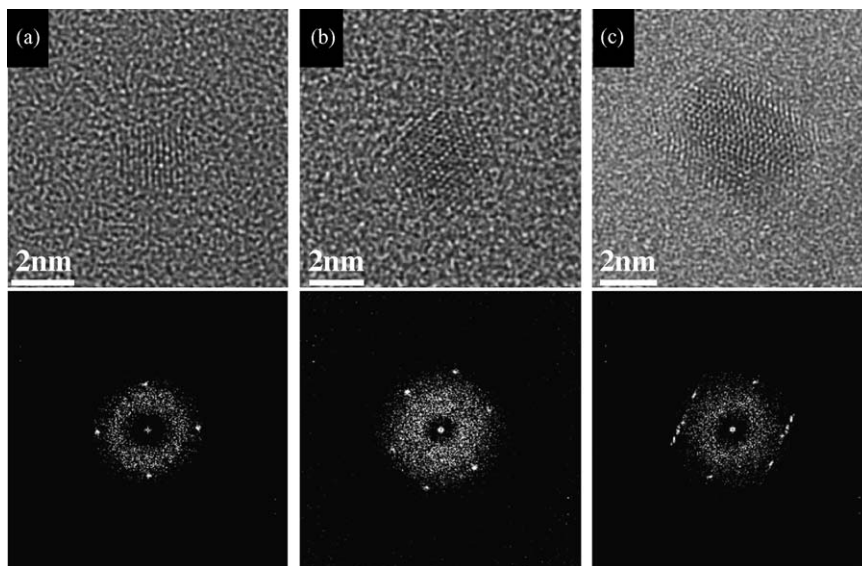
Fig. 7. HRTEM images of particles observed in the samples prepared with pH 5 with their corresponding FFTs. Three small particles show fringe contrasts (a–c) and a well defined hexagonal contrast (b).

the samples obtained at pH 5 and pH 6 demonstrate a higher reduction rate for higher pH values and formation of bigger Zn clusters.

Considering all the parameters studied, we can identify a strong relation between the pH conditions and the size distribution of the Zn nanoparticles and also the aggregation process during the synthesis as the following:

At the pH value 3, the particles are formed in a slow process that reduces the ions slowly and tend to search for minimal energy surfaces, implying an aggregation process similar to a nucleation behavior. Therefore, the twins appear when the aggregation is not regular and the internal strain energy

searches the way to be released. This behavior produces well-passivated clusters, but because of the low velocity of reaction, the size distribution is not well controlled.

For pH 4, the reduction is more efficient but the presence of free ions and electrons in the solution generate more particles of smaller size after the initial nucleation process, causing aggregation of relatively fewer particles to generate particles with worse defects. The reduction at pH 5 is fast and produces zinc particles of 2.5 nm average size with the smallest observed dispersion, reducing most of the metal ions in the reaction solution. The use of pH 6, besides strong reduction, induces strong aggregation of particles, which might be due to weak coordination of tannin in the biomass
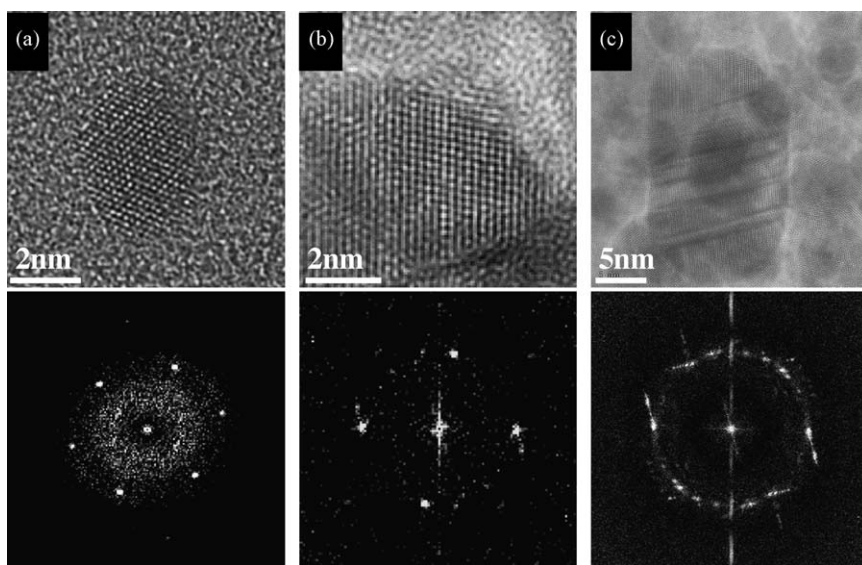
Fig. 8. HRTEM images of particles in the samples prepared with pH 6: (a) a hexagonal particle in {0 0 1} orientation, (b) a rhombic contrast of a hexagonal particle; and (c) multiple particles including a nanorod of 12 and 25 nm of wide and length, respectively. Corresponding FFTs are shown at the bottom.
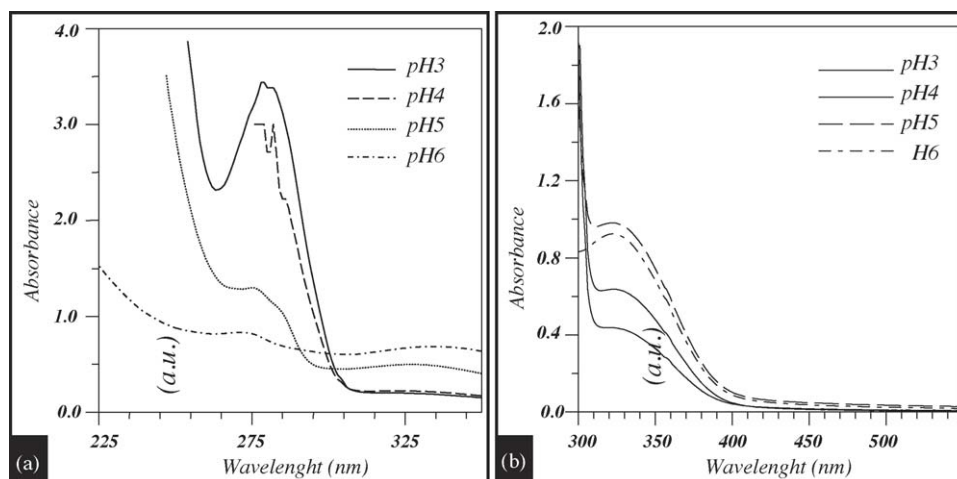
Fig. 9. Optical absorbance for the samples obtained at different pH values: (a) evidences of free Zn^+ ions in different samples; and (b) SPR band related to the formation of Zn quantum clusters.

with Zn, leaving free Zn^0 atoms in the solution. The free Zn^0 atoms coalesce with the already formed clusters under the soft surfactant tannin forming Zn nanorods. Until we know, this is the first evidence of Zn nanorods formation.

4. Conclusions

The bio-reduction method using different pH conditions proved to be a powerful method for obtaining a large amount of Zn nanoparticles in different configurations and sizes. Apart from the efficiency of reduction of the Zn^{2+} ions, the pH of the reaction solution has a direct influence in the size, structure and homogeneity of the small nanoparticles. It was identified that reduction at pH 5 produces the smallest and less dispersed Zn nanoparticles, while the use of pH 6 makes the reduction process very fast, causing fast aggregation of nanoparticles and leaving extra Zn atoms in the solution to generate small nanorods growing in preferential directions. The structure of the obtained Zn nanoparticles is preferentially hexagonal as is the symmetry of the bulk crystal; however the samples showed also multiple-twinned clusters when they were obtained at pH 3 and pH 6. The existence of a few particles with fcc-like structure was identified. The use of theoretical methods for stability and HRTEM image simulation helped to improve the experimental data interpretation.

Through this work, we demonstrate the efficiency of bio-reduction technique for the size and structure controlled synthesis of small Zn nanoparticles in the quantum-dot range, which may open-up the possibility of using them in optical and electronic devices.

Acknowledgements

References

[1] Z. Tang, N.A. Kotov, M. Giersig, Science 297 (2002) 237.
[2] S. Botti, R. Coppola, F. Gourbilleau, R.P. May, R. Rizk, M. Valli, Appl. Phys. A 74 (2002) s1230.
[3] Ch.T. Campbell, S.C. Parker, D.E. Starr, Science 298 (2002) 811.
[4] A.T. Bell, Science 299 (2003) 1688.
[5] D.F. Emerich, C.G. Thanos, Exp. Opin. Biol. Ther. 3 (2003) 655.
[6] Z.W. Pan, Z.R. Dai, Z.L. Wang, Science 291 (2001) 1947.
[7] L.F. Dong, Z.L. Cui, Z.K. Zhang, Nanostruct. Mater. 8 (1997) 815.
[8] Y. Yan, P. Liu, J.G. Wen, B. To, M.M.J. Al-Jassim, Phys. Chem. B 107 (2003) 9701.
[9] J. Wang, G. Wang, J. Zhao. Phys. Rev. A 68 (2003) 013201.
[10] F. Rataboul, C. Nayral, M.J. Casanove, A. Maisonnat, B. Chaudret, J. Organomet. Chem. 643 (2002) 307.
[11] J. Gardea-Torresday, K. Tiemman, G. Gamez, K. Dokken, S. Tehuacanero, M. Jose-Yacaman, J. Nanoparticles Res. 3 (2001) 475.
[12] G. Canizal, J.A. Ascencio, J. Gardea-Torresday, M. José-Yacamán, J. Nanoparticles Res. 3 (2001) 475.
[13] J.A. Ascencio, Y. Mejia, H.B. Liu, C. Angeles, G. Canizal, Langmuir 19 (2003) 5882.
[14] J.A. Ascencio, A.C. Rodríguez-Monroy, H.B. Liu, G. Canizal, Chem. Lett. 33 (2004) 1056.
[15] P. Mukherjee, A. Ahmad, D. Mandal, S. Senapati, S.R. Sainkar, M.I. Khan, R. Ramani, R. Parischa, P.V. Ajayakumar, M. Alam, M. Sastry, R. Kumar, Angew. Chem. 40 (2001) 3585.
[16] J.A. Ascencio, C. Gutiérrez-Wing, M.E. Espinosa-Pesqueira, M. Marín, S. Tehuacanero, C. Zorrilla, M. José-Yacamán, Surf. Sci. 396 (1998) 349.
[17] J.F. Sánchez-Ramírez, C. Vazquez-Lopez, U. Pal, Sup. Vac. 15 (2002) 16.
[18] P. Mulvaney, Langmuir 12 (1996) 788.
[19] DMol3 Module of Cerius2, Accelrys, San Diego, 1999.
[20] B. Delley, J. Chem. Phys. 113 (2000) 7756.
[21] J.P. Perdew, Y. Wang, Phys. Rev. B 45 (1992) 13244.

[22] D. Tomanek, A.A. Aligia, C.A. Balseiro, Phys. Rev. B 32 (1985) 505.

[23] F. Cleri, V. Rosato, Phys. Rev. B 45 (1993) 22.

[24] J. Riffkin, Center for Simulation, University of Connecticut, USA, http://ims.uconn.edu/centers/simul.

[25] K. Widder, M. Knupfer, O. Knauff, J. Fink, Phys. Rev. B 56 (1997) 10154.

[26] M. Jose-Yacaman, J.A. Ascencio, S. Tehuacanero, M. Marin, Top. Catal. 18 (2002) 167.

[27] M. Jose-Yacaman, S. Tehuacanero, C. Zorrilla, J.A. Ascencio, A. Gómez, Nanostruct. Mater. 10 (1998) 1.

[28] J.A. Ascencio, M. Mendoza, T. Santamaria, M. Perez, I. Nava, C. Gutiérrez-Wing, M. José-Yacamán, J. Clust. Sci. 13 (2002) 189.

[29] H.B. Liu, M. Jose-Yacaman, R. Perez, J.A. Ascencio, Appl. Phys. A 77 (2003) 63.

[30] C. Gutiérrez-Wing, J.A. Ascencio, W. De la Cruz, L. Cota, M. José-Yacamán, J. Nanosci. Nanotech. 2 (2002) 101.